Large-eddy simulations of interaction between surface waves and a tidal turbine wake in a turbulent channel

T. Stallard[1], H. Mullings[1], S. Draycott[1], P. Ouro[1]

Abstract—**Most deployment sites for tidal stream turbines feature relatively shallow conditions and are typically exposed to surface waves, which can drive periodic loads on the turbine as well as change the recovery dynamics of the turbine wake depending on their characteristics. This paper presents results of high-fidelity large-eddy simulations with an actuator-line method of a horizontal axis tidal stream turbine subjected to deep water waves and compared to no-wave, current only conditions. Results show that under periodic wave conditions, the turbine wake recovery is more rapid than in the absence of waves over a distance of up to 45 diameters downstream with the largest differences of velocity deficit observed at a streamwise distance ranging from 15 to 30 diameters. The waves increase the vertical mixing and enhance the breakdown of tip vortices, which are non-uniformly advected due to the wave-induced variation of velocity in the region of flow between the turbine top-tip and free-surface. Power spectral density of the turbine rotor thrust reveals a larger energy peak at wave frequency than blade passing frequency, thus playing a large role in modulating turbine load variation.**

Index Terms—**Tidal turbine arrays, Large-eddy simulation, Bathymetry, Wakes**

I. Introduction

TIDAL stream turbines are now being developed for array deployments, largely at sites with relatively shallow water depths on either bed-supported or floating support structures [1]. Whilst proximity to the free-surface offers the largest availability of kinetic energy to be harnessed, this location in the water column also presents design challenges with increased exposure to wave-induced kinematics leading to potential for increased peak- and fatigue-loads [2]–[4] and enhanced occurrence of flow separation [5]. The latter are also applicable to bottom-fixed turbines but to a lesser extent, i.e. for a narrower band of wave conditions, with bathymetry-induced turbulence presenting a more onerous challenge for these designs [6], [7]. From a flow hydrodynamics perspective, ocean waves also have the ability to alter turbine wake recovery rate as they induce vertical mixing and introduce a pulsatile streamwise flow that impacts the coherence of the wake structure and dynamics of turbine loading [8]. Thus, understanding of how waves change the local flow dynamics can influence the siting of tidal stream turbine arrays and operation of turbines, and are also an important load case for the design of turbines and the supporting structure or moorings of floating systems [9].

To-date the impact of waves on turbine loading and on wake recovery has received limited attention, generally for specific combinations of conditions reproducible in experimental facilities [10]–[13] or numerical models [14]–[16]. A challenge to reproduce combined wave-current conditions is that the experimental facilities are required to have large dimensions so that wave reflection or other phenomena are minimum, especially when studying the velocity field. In addition, measuring the instantaneous velocity field when the free-surface is moving is challenging.

The numerical simulation of wave-current conditions is extremely challenging as the air-water interface needs to be resolved with accuracy at the same time as the turbulent flow scales are resolved, e.g. those in the approach flow or induced by the rotating turbine or bathymetry features. Three main numerical techniques can be used in Computational Fluid Dynamics (CFD) models in the Eulerian framework to account for free-surface effects, namely arbitrary Lagrangian-Eulerian (ALE) approaches that deform the mesh according to the resulting free-surface motion [16], Volume of Fluid (VoF) methods that resolve a continuum colouring function that indicates the fraction of air and liquid in every cell [14]; and Level-Set Method (LSM) techniques that resolve the advection equation for a continuous signed function that represents the fluid interface [17]. The advantage of the last two methods is that the mesh does not change in time, avoiding computationally expensive mesh conforming operations. However, these approaches do require that the air portion is also modelled, even though this region does not have

Tim Stallard. Professor of Offshore and Renewable Energy Engineering. School of Engineering, University of Manchester, Manchester, M13 9PL, UK (e-mail: tim.stallard@manchester.ac.uk).

Hannah Mullings. Research Associate. School of Engineering, University of Manchester, Manchester, M13 9PL, UK (e-mail: hannah.mullings@manchester.ac.uk).

Samuel Draycott. Dame Kathleen Ollerenshaw Research Fellow. School of Engineering, University of Manchester, Manchester, M13 9PL, UK (e-mail: samuel.draycott@manchester.ac.uk).

Pablo Ouro. Dame Kathleen Ollerenshaw Research Fellow. School of Engineering, University of Manchester, Manchester, M13 9PL, UK (e-mail: pablo.ouro@manchester.ac.uk).

This work was supported by the Tidal Stream Industry Energiser Project (TIGER), a European Union INTERREG V A France (Channel) England Research and Innovation Programme, which is co-financed by the European Regional Development Fund (ERDF), and by the EPSRC Offshore Renewable Energy Hub (EP/S000747/1). The simulations used the ARCHER2 UK National Supercomputing Service (https://www.archer2.ac.uk).

Affiliations: (1) School of Engineering, University of Manchester, UK.

Digital Object Identifier:
https://doi.org/10.36688/ewtec-2023-503

direct relevance to tidal flows and increases the overall number of grid points simulated. LSM allows to capture the actual deformation of the free-surface but at a higher computational expense than VoF. Alternative to Eulerian methods are the Lagrangian or particle-based methods that handle well free-surface flows [18] but without an accurate resolution of the turbulent field.

Previous studies [14], [16] have looked into uniform inflow conditions with waves using the Reynolds-Averaged Navier Stokes (RANS) approach, valuable to infer load variation on the turbine but with medium fidelity when accounting for the wave effects on the wake recovery due to turbulence not being resolved [19]. To this end, the turbulence closure of Large-Eddy Simulation allows to resolve the turbulent turbine wake [20] and flow structures larger than the grid size, thereby increasing model accuracy [21], especially useful to compute unsteady loading to estimate fatigue behaviour [22]. With the explicit resolution of the velocity field, the flow mechanisms responsible for the wake recovery can be quantified [23] and thus evaluate the effect of ocean waves.

This paper presents the first set of simulations using an in-house large-eddy simulation code with a level-set method for resolving the air-water interface and actuator-line method for the turbine rotor blades representing a single horizontal axis turbine subject to turbulent flow co-existing with waves. Comparisons with a no-wave case enables the quantification of the role of waves on the studied setup and motivates the further study of a wider set of conditions to unveil how ocean waves will drive tidal stream turbine loads and wake recovery and to assess the modification of waves as they propagate over the wake region.

II. DOFAS: IN-HOUSE LES SOLVER

The Digital Offshore FArms Simulator (DOFAS) is an in-house large-eddy simulation (LES) code that adopts the spatially-filtered Navier-Stokes equations to explicitly resolve the turbulent scales larger than a given filter size, in this case this is the grid size. In LES, a sub-grid scale model is adopted to model the flow structures smaller than the grid size, which is normally considered to be isotropic turbulence as they have relatively low energy content. Herein the Wall-Adapting Local-Eddy viscosity (WALE) model from [24] is adopted as it does not require an explicit treatment in the turbulent viscosity in proximity of boundaries, e.g. free-surface as in this study. The numerical domain is discretised into a rectangular Cartesian grid with staggered storage of velocities. An explicit fractional-step method is adopted to advance the simulation in time, with a multi-grid to resolve the Poisson pressure equation.

Hydrodynamically smooth and rough wall functions are available in DOFAS to allow the use of relatively large grid resolutions near the walls, alleviating the demand for large computing resources. Surface waves can be explicitly simulated in DOFAS with a Level-Set Method (LSM) adopting linear or second-order Stokes theories. At the inlet, a Dirichlet boundary condition is set in terms of wave-induced and vertical shear distribution velocities as well as establishing the instantaneous free-surface elevation. At the outlet, an absorption layer is at the outlet in order to avoid wave reflections [17].

DOFAS uses an Actuator Line Method (ALM) to resolve the rotating turbine rotor's blades with a Prandtl correction to account for tip losses, or with a non-rotating Actuator Disc Method (ADM). The use of ALM or ADM allows to have relatively coarse grid resolutions without the need for explicitly resolving the rotor geometry, which alleviates the inherent computational cost of performing LES [9]. Ouro et al. [21] validated the accuracy of the LES-ALM method in DOFAS in terms of hydrodynamic coefficients and turbulent flow statistics in the wake up to 8D downstream of small-scale tidal turbine arrays. The parallel implementation of the ALM in DOFAS, enables the modelling of dozens of turbines in a computationally efficient way [25]. Ouro et al. [26] performed the LES of several aligned and staggered array layouts with DOFAS, showing that staggered configurations are less sensitive to turbine spacing than aligned layouts, with the former yielding larger energy output due to the bypass flow generated between upstream turbines.

III. NUMERICAL SETUP

A single prototype-scale tidal stream turbine is simulated keeping the same dimensions as in the experimental campaign described in Stallard et al. [10]. The turbine's diameter (D) is 0.27 m with axis (z_{hub}) located at mid water depth equal to 0.225 m and at a distance of 8.36 m from the inlet. The device operates at peak power coefficient achieved at tip-speed ratio of approx. 4.5, equivalent to a rotational speed of 15.33 rad/s based on the bulk velocity (U_0) equal to 0.47 m/s. The mean water depth (H) is equal to 0.45 m. A schematic of the computational domain is presented in Fig. 1 in which the logarithmic velocity distribution [27] is imposed at the inlet with a friction velocity of 0.0187 m/s is represented. At the inlet, artificial turbulence is superimposed to the mean velocity profile using an anisotropic version of the Synthetic Eddy Method [28] with a turbulence intensity of 10% and lengthscale of 0.2 m, 0.1485 m and 0.1125 m in x-, y- and z-directions, respectively.

Two simulations are presented here, namely a no-wave case in which only vertical shear and artificial turbulence are imposed at the inlet, and a wave case that also considers periodic deep-water waves with a height (h) of 0.05 m, non-dimensional wavenumber (kh) equal to 2.827, and frequency of 1.715 Hz. The wavelength, λ, is therefore 1 m. These wave characteristics have been adopted so they represent short, approximately deep-water waves and provides a ratio of turbine rotational frequency to that of waves of approx. 0.7, i.e. there is potential for the interaction between wave frequency harmonics and rotational effects from the turbine. Note that the turbine is set to rotate at constant speed without any controller included despite the fact that control can be used to reduce structural

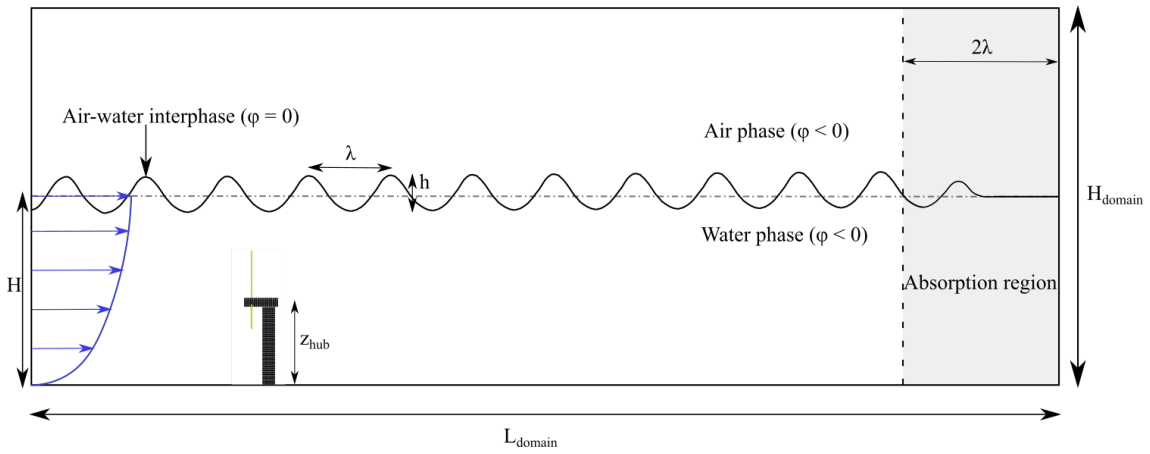

Fig. 1. Schematic of the numerical domain considered in the LESs.

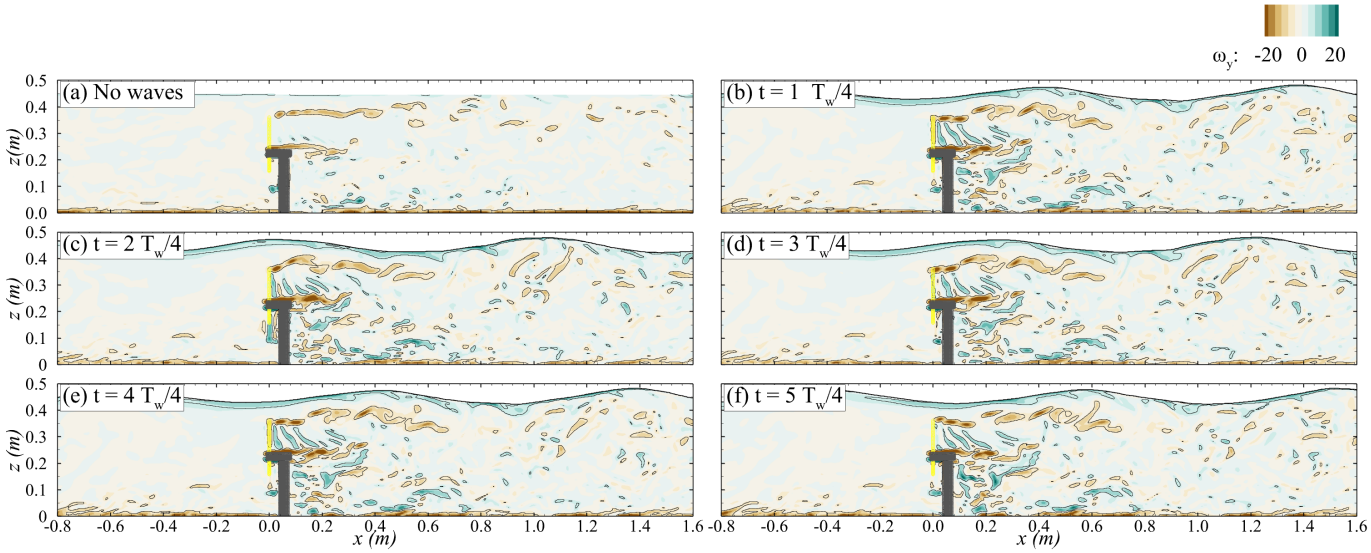

Fig. 2. Vertical plane of spanwise vorticity (ω_y) field along centreline of device for the current only (a) case and at five instants during a wave cycle for the wave case (b) to (f).

loads. In both cases the free-surface motion is solved with the LSM so that velocity-induced changes to the air-water interface are captured even for the no-wave case.

The numerical domain is set to measure 20 m long and 3 m wide, which is larger in its streamwise dimension (L_{domain}) than the experimental open-channel flow facility [10] in order to avoid any reflection from the waves, allowing regions of wave development (upstream of the turbine with about a length of about 8λ), turbine wake recovery (whose length extends approx. 10λ) and wave absorption (final downstream region measuring 2λ). The total height (H_{domain}) is 1.2 m which is about 2.6 times the water depth (H) to avoid any interaction of the upper boundary condition in the free-surface development.

A uniform grid resolution of 0.005 m is adopted across the entire domain (as required to solve the LSM in DOFAS), with fixed time step of 0.001 s as previously adopted for the validation of DOFAS [21] for the same experimental case in current-only conditions. Simulations are run on ARCHER2, the UK national supercomputing facility, adopting 8,000 cores. A total physical time of 400 s is run, with first-order statistics collected after 50 s and second order statistics after another 100 s for a total of 250 s.

IV. Results

The impact of periodic surface waves on an operating tidal stream turbine is analysed based on instantaneous spanwise vorticity contours to visualise the tip vortex generation and their convection downstream, and also by looking at the mean wake hydrodynamics to infer whether wake recovery is faster or slower for these set of flow conditions.

A. Instantaneous flow field

Figure 2 presents the contours of instantaneous spanwise vorticity field over a vertical plane through the centre of the turbine for a single time instant of the no-wave case (Fig. 2(a)) and five snapshots of the wave case covering a wave cycle of duration T_w equal to 0.583 s. The simulated waves approach deep-water conditions and change the convection pattern of the tip vortices once shed by the turbine blades when close to the free-surface. During the period of wave

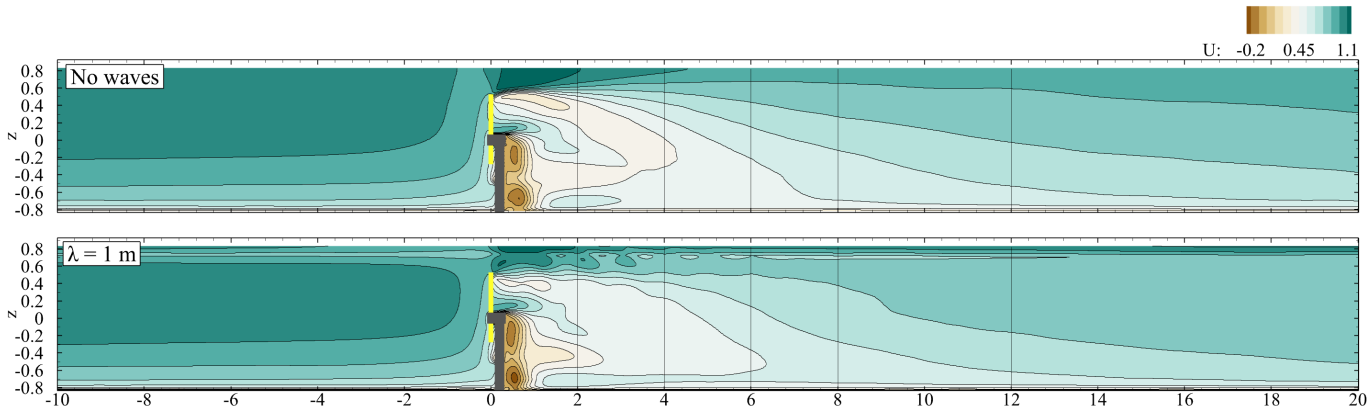

Fig. 3. Contours of the mean streamwise velocity for the no-wave (top) and wave (bottom) cases.

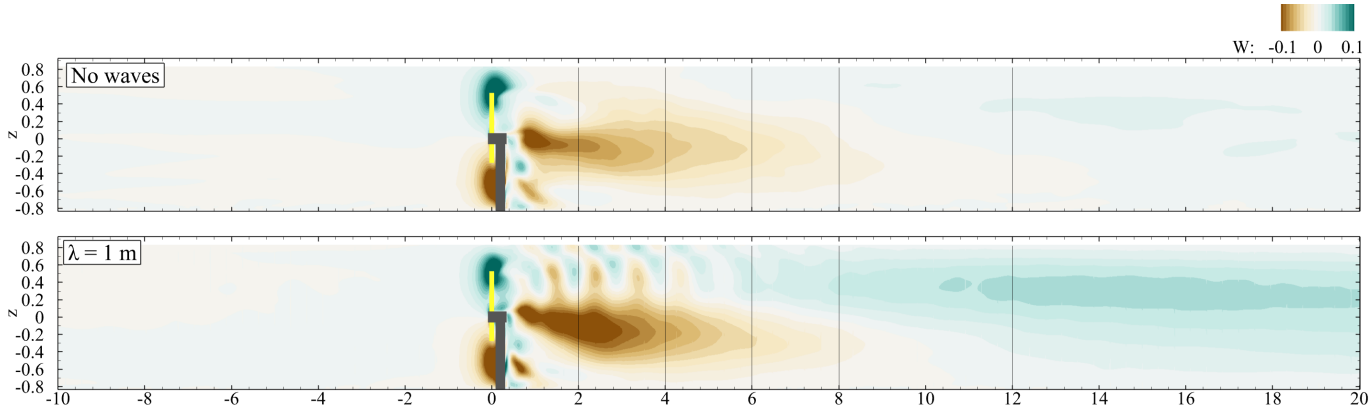

Fig. 4. Contours of the mean vertical velocity for the no-wave (top) and wave (bottom) cases.

trough-to-crest, the reduction in velocities near the free-surface prevents these turbulent structures to be shed downstream in a periodic and equally-distanced manner [29], [30], eventually creating a region in which these flow structures are clustered, as seen in Fig. 2 (a) and (f). As the waves travel downstream and their crest moves towards the turbine location, the wave-induced velocities increase and lead to the downstream convection of the shed tip vortices, as shown in Fig. 2 (b). At this stage, the separation between the tip-vortices also increases when compared to the no-wave case (Fig. 2(a)), as the local velocities are higher. The coherence of the tip vortices is lost after a distance of approx. 0.8 m, i.e. approximately three turbine diameters downstream.

During these conditions the turbine actually operates with a variable tip-speed ratio as the onset flow speed constantly changes. To develop constant blade load through a wave cycle as observed in the no-wave case, control would need to be applied to either blade pitch angle or rotor angular speed, throughout each wave cycle. However, for such short waves this is not trivial and a fixed pitch and constant angular speed are applied in these simulations.

In Fig. 2 (c) and (d) it is observed that the vertical location of the tip vortices is not aligned with the top-tip location, as waves induce a vertical velocity field which moves vortices upwards in phase with the free-surface elevation and downwards when going from wave crest to trough. This eventually increases the vertical mixing of the turbulent flow that accelerates the loss of coherence of tip vortices and thus promoting a faster wake recovery, as shown later.

The instantaneous vorticity contours shown in Fig. 2 (b) to (f) for the wave case also show that vortical structures remain close to the free-surface layer, suggesting that turbine-induced turbulence can somehow alter the wave dynamics.

B. Mean velocity field

The distribution of the time-averaged streamwise velocity field across the centre of the channel is shown in Fig. 3 for both cases. Similar inflow conditions are observed independently to the wave condition, with only a slight deceleration near the free-surfrace about two diameters upstream of the turbine. Immediately after the turbine top-tip, there is a flow acceleration region seen in the no-wave case whilst this is less clear in the wave cases. In the latter intermittent regions of higher velocities are observed almost until six diameters downstream near the free-surface.

Contours with mean vertical velocity distribution are presented in Fig. 4. Immediately downstream of the turbine rotor, for the current-only case there is a predominant negative vertical velocity at hub height extending further until about six diameters downstream. When waves are introduced, there is a change in the W pattern near the top-tip height with alternative regions of positive and negative velocities. Behind the turbine's hub, the negative vertical velocity region is

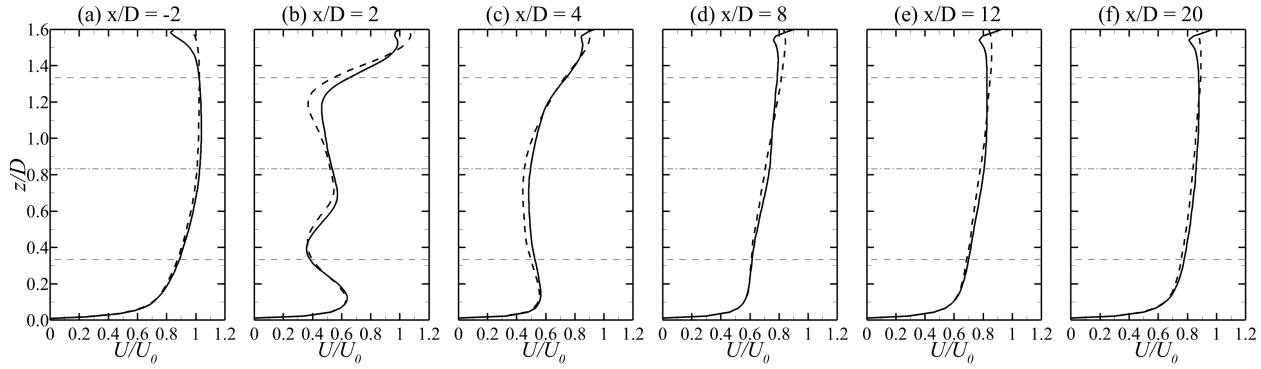

Fig. 5. Vertical profiles of normalised mean streamwise velocity U/U_0 at various downstream distances for the no-wave (dashed line) and wave (solid line) cases.

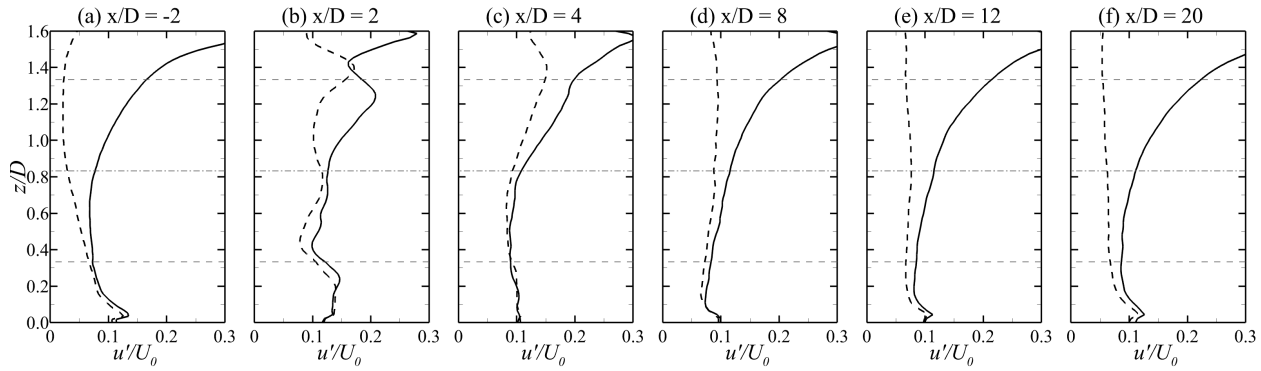

Fig. 6. Vertical profiles of mean streamwise velocity fluctuations (u'/U_0) at various downstream distances for the no-wave (dashed line) and wave (solid line) cases.

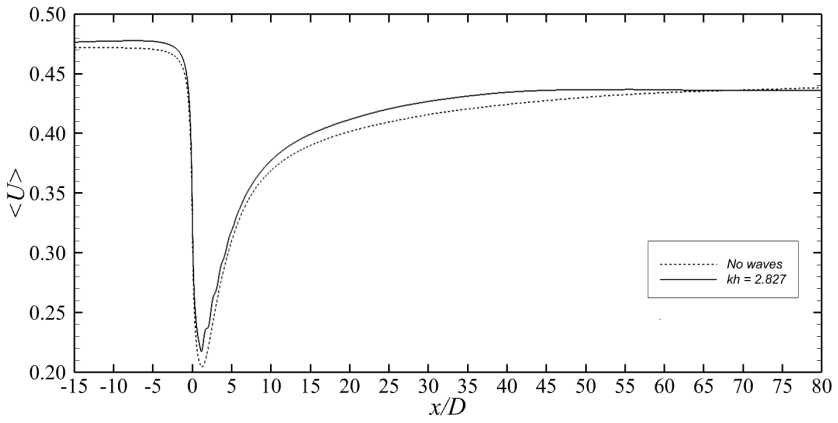

Fig. 7. Streamwise evolution of the disc-averaged mean streamwise velocity $< U >$ upstream and downstream of the turbine for the no-wave and wave case.

more pronounced than in the no-wave case whilst in the far wake, after about 10 diameters downstream, a positive vertical velocity component dominates over the entire water depth. The latter is also observed in the no-wave case but with a lower velocity magnitude.

Results of the mean velocity field presented in Fig. 3 and 4 indicate that the simulated deep-water waves change the near-wake by an enhanced vertical mixing also aided by the quicker loss of coherence of the tip vortices seen in Fig. 2.

C. Vertical profiles

Profiles with the vertical distribution of normalised mean streamwise velocity U/U_0 over the centre of the wake (y/D = 0) at two diameters upstream of the turbine and various downstream distances is presented in Fig. 5 for both wave and no-wave cases. Upstream flow conditions to the turbine, the logarithmic velocity profile is developed independently to the wave condition, whilst the fluctuating streamwise kinetic energy shows an exponential decay from a maximum of approx. u'/U_0 = 0.3 near the mean water level until a height of z/D = 0.35 at which this follows the values from the no-wave case. Immediately downstream of the turbine, at x/D = 2, the time-averaged velocity is dominated by the influence of the turbine, with the two low-velocity regions near the bottom and top-tip locations. In absence of waves, the velocity near

the top-tip recovers at a slower pace as waves induce a higher vertical mixing, observed from the instantaneous vorticity contours presented in Fig. 2. At x/D = 4, the velocity profile is very similar between cases with a slight lower velocity between hub and bottom-tip height for the no-wave case. Further downstream, after $x/D \geq$ = 8, the vertical distribution of U/U_0 remains similar independently of the wave condition, albeit there are higher velocities near the free-surface in the no-wave case.

Figure 6 shows the vertical distribution of mean streamwise velocity fluctuations over the wake centre at the same downstream stations as in Fig. 5. At x/D = 2, the waves largely distort the distribution of the fluctuation of velocities over the water depth, increasing its values from the no-wave case over nearly the entire water depth, i.e. from the turbine bottom-tip location until the free-surface, as a result of the increased vertical mixing. Further downstream, it is observed that waves include a large change to the time-averaged unsteady velocity field near the free surface. At x/D = 4, the deviation between the wave and no-wave cases starts at about $0.4D$ from the channel bed, whilst after x/D = 12 downstream of the turbine, the impact of the waves on the u' field is observed from the bed bottom.

D. Wake recovery

The rotor-averaged velocity is computed both upstream and downstream of the tidal turbine and values are shown in Fig. 7 for the wave case and current-only flow conditions. The velocity magnitude approaching the turbine is slightly higher for the wave case. Downstream of the turbine, the disc-averaged velocity seems to be turbine-dominated, i.e. independent to the presence of the waves, up to 8–10 diameters. After a distance of approx. $10D$ behind the turbine, there is a quicker velocity recovery for the wave case likely due to the higher wake mixing through the water column, as shown previously. After 55–60 diameters downstream, i.e. in the very far wake, the disc-averaged velocity converges for both simulated cases but with a value lower than the bulk velocity.

The spatial distribution of the mean streamwise velocity over transverse cross-sections are presented in Fig. 8 at x/D = 4, 8 and 20. In the near wake, it is observed that the velocity deficit region is mostly enclosed within the swept area for both cases, as seen in the vertical profile in Fig. 5 at x/D = 2, as this is the turbine-dominated wake region with minor impact from the waves on the mean wake. Further downstream at x/D = 8, the waves lead to lower velocities near the free surface and transverse wake expansion, whilst similar velocity distribution is seen below hub height. In the far-wake, at x/D = 20, near the mean water depth elevation, the velocities are lower for the wave cases, with the high velocity regions found almost between bottom- and top-tip heights whilst for the no-wave case these are found closer to the free-surface. Such differences in mean velocity distribution supports the downstream evolution of the disc-averaged value presented in Fig. 3.

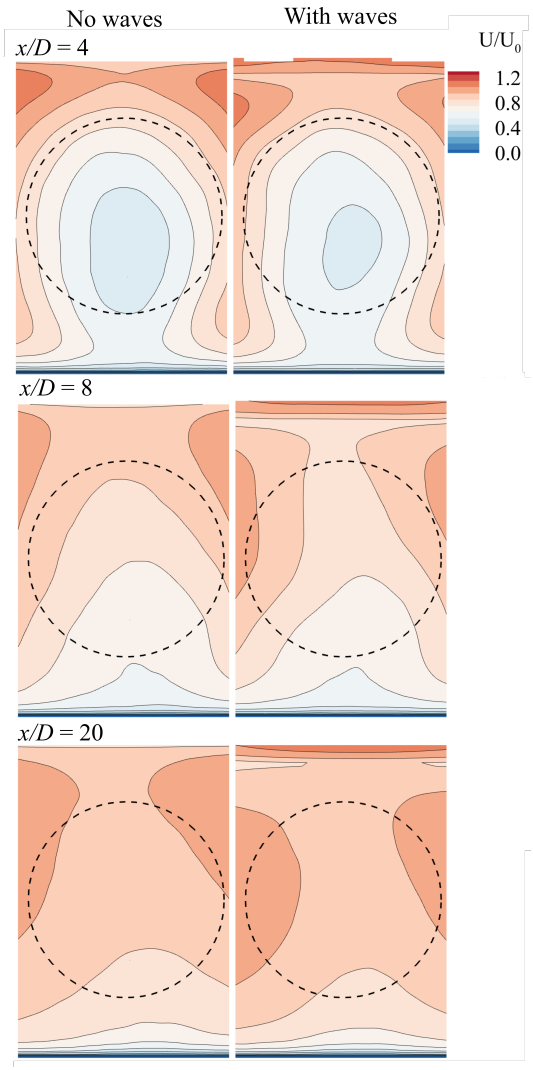

Fig. 8. Cross-section at x/D = 4 with contours of normalised mean streamwise velocity for the (left) no-wave and (right) wave cases.

E. Spectra of velocity and turbine thrust

To elucidate the impact of waves on the instantaneous loading of the tidal stream turbine, in Fig. 9 the Power Spectral Density (PSD) of the turbine rotor thrust time series and vertical velocity fluctuation sampled at two diameters upstream of the turbine at hub height, with the frequency normalised by the rotational frequency of the turbine (f_T). In the no-wave case, the PSD of the thrust force features an energy peak at the blade passing frequency, i.e. at 3 f_T. In the presence of deep-water waves, the wave frequency is identified from the velocity time series at about 0.7 f_T, which the subsequent peak in the thrust PSD at that frequency. This peak is larger than that at the blade passing frequency, indicating that waves play a larger role in modulating the loading dynamics that the actual rotation of the turbine through the vertical shear velocity profile. A harmonic of the wave frequency is observed at about 1.4 f_T with subsequent harmonics not identified likely to be interfering with the blade passing frequency peak and its own harmonics. These LES results agree very well with those recently shown by Zang et al. [13] with a laboratory experiment.

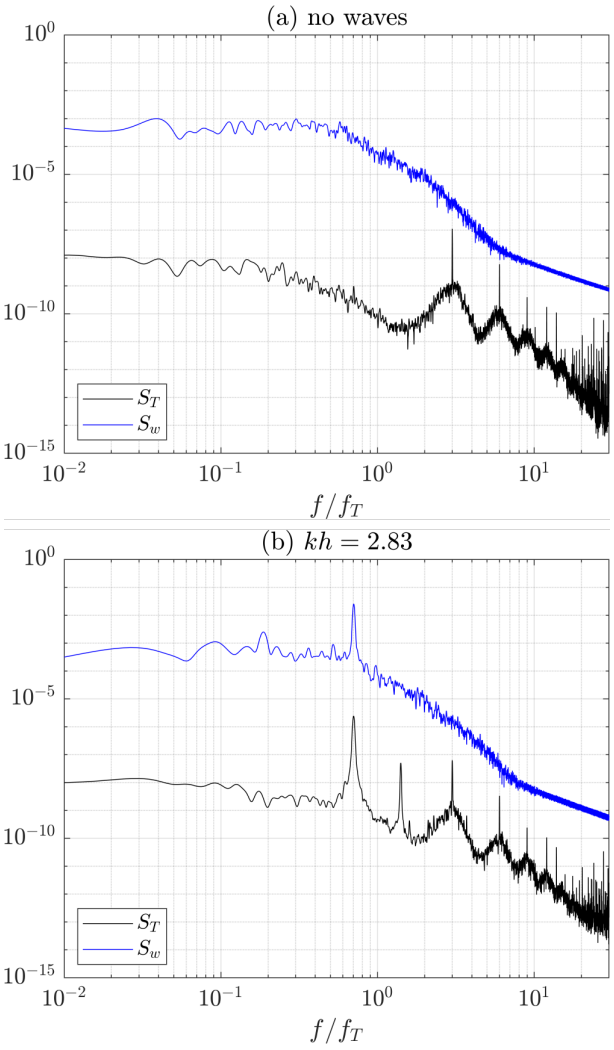

Fig. 9. Power Spectral Density of the turbine rotor thrust and vertical velocity fluctuation sampled at hub height two diameters upstream of the turbine for the (a) current-only and (b) wave cases.

V. Discussion and Conclusions

This paper presents large-eddy simulations of a single horizontal axis tidal stream turbine operating in a turbulent open-channel flow in shear current-only conditions and also including following surface waves that approach deep-water conditions. Results show that the periodic nature of waves causes a large change in the convection of the tip vortices in the near wake. In particular whilst the surface elevation reduces above the turbine, the lower convection velocity near the free-surface leads to a clustering effect of the tip vortices. These are eventually convected downstream whilst the surface elevation above the turbine increases towards a crest and velocities increase.

Waves increase the vertical mixing over almost the entire water column (as the non-dimensional wavenumber, kh with H denoting mean water depth, is 2.83), which leads to a quicker momentum recovery in most of the wake region after about eight diameters downstream of the turbine. This is observed in the downstream evolution of the disc-averaged mean streamwise velocities and contours of mean velocity over transverse cross-sections over the wake. After a distance of about 55 to 60 diameters downstream, the disc-averaged velocity in the wake for both cases converges to a similar value.

The waves studied, with wavelength 1 m ($0.45H$) and height 0.05 m ($0.11H$), are observed to alter the rate of wake recovery, increasing the rate in the near-wake of the turbine and slightly reducing the rate beyond eight diameters downstream. Analysis of the streamwise kinetic energy, due to turbulence of the flow and the wake combined with the periodic variation due to the surface waves, indicates a significant variation across the water column due to wave action with the wave induced kinematics extending to about 0.4D from the bed until about six diameters downstream. Power spectral density of the thrust force for the wave case highlighted the wave signature on turbine loading, with largest energy peak at the wave frequency.

Further research should assess the impact of waves with different characteristics on the turbine's loading and dynamics of wake recovery , as well as the potential distortion to the wave field due to turbine-induced flow changes.

References

[1] L. Perez, R. Cossu, A. Grinham, and I. Penesis, "Seasonality of turbulence characteristics and wave-current interaction in two prospective tidal energy sites," *Renewable Energy*, vol. 178, pp. 1322–1336, 2021.

[2] P. W. Galloway, L. E. Myers, and A. B. S. Bahaj, "Quantifying wave and yaw effects on a scale tidal stream turbine," *Renewable Energy*, vol. 63, pp. 297–307, 2014.

[3] S. C. Tatum, C. H. Frost, M. Allmark, D. M. O'Doherty, A. Mason-Jones, P. W. Prickett, R. I. Grosvenor, C. B. Byrne, and T. O'Doherty, "Wave-current interaction effects on tidal stream turbine performance and loading characteristics," *International Journal of Marine Energy*, vol. 14, pp. 161–179, 2016.

[4] H. Mullings and T. Stallard, "Analysis of tidal turbine blade loading due to blade scale flow," *Journal of Fluids and Structures*, vol. 114, p. 103698, 2022.

[5] G. T. Scarlett, B. Sellar, T. van den Bremer, and I. M. Viola, "Unsteady hydrodynamics of a full-scale tidal turbine operating in large wave conditions," *Renewable Energy*, vol. 143, pp. 199–213, 2019.

[6] P. Ouro and T. Stoesser, "Impact of Environmental Turbulence on the Performance and Loadings of a Tidal Stream Turbine," *Flow, Turbulence and Combustion*, vol. 102, pp. 613–639, 2019.

[7] P. Mercier, M. Grondeau, S. Guillou, J. Thiébot, and E. Poizot, "Numerical study of the turbulent eddies generated by the seabed roughness. Case study at a tidal power site," *Applied Ocean Research*, vol. 97, p. 102082, 2020.

[8] S. Draycott, G. Payne, J. Steynor, A. Nambiar, B. Sellar, and V. Venugopal, "An experimental investigation into non-linear wave loading on horizontal axis tidal turbines," *Journal of Fluids and Structures*, vol. 84, pp. 199–217, 2019.

[9] P. Stansby and P. Ouro, "Modelling marine turbine arrays in tidal flows," *Journal of Hydraulic Research*, vol. 60, pp. 187–204, 2015.

[10] T. Stallard, R. Collings, T. Feng, and J. Whelan, "Interactions between tidal turbine wakes: experimental study of a group of three-bladed rotors," *Philosophical Transactions of the Royal Society A: Mathematical, Physical and Engineering Sciences*, vol. 371, p. 20120159, 2013.

[11] S. Draycott, J. Steynor, A. Nambiar, and V. Sellar, B. nd Venugopal, "Rotational sampling of waves by tidal turbine blades," *Renewable Energy*, vol. 162, pp. 2197–2209, 2020.

[12] Y. Zhang, W. Zang, J. Zheng, L. Cappietti, J. Zhang, Y. Zheng, and E. Fernandez-Rodriguez, "The influence of waves propagating with the current on the wake of a tidal stream turbine," *Applied Energy*, vol. 290, p. 116729, 2021.

[13] W. Zang, Y. Zhang, Y. Zeng, J. Zhang, D. Guan, and E. Fernandez-Rodriguez, "On the impact of waves and turbulence on the power fluctuations and wake structure of a tidal-stream turbine," *Physics of Fluids*, vol. 34, p. 055115, 2023.

[14] D. Apsley, T. Stallard, and P. Stansby, "Actuator-line CFD modelling of tidal stream turbines," in *CORE2016 - 2nd International Conference on Offshore Renewable Energy*, 2016.

[15] S. F. Sufian, M. Li, and B. A. O'Connor, "3D modelling of impacts from waves on tidal turbine wake characteristics and energy output," *Renewable Energy*, vol. 114, pp. 308–322, 2017.
[16] Z. Li, K. Ghia, Y. Li, Z. Fan, and L. Shen, "Unsteady Reynolds-averaged Navier–Stokes investigation of free surface wave impact on tidal turbine wake," *Proceedings of the Royal Society A: Mathematical, Physical and Engineering Sciences*, vol. 477, p. 20200703, 2021.
[17] A. Christou, Z. Xie, T. Stoesser, and P. Ouro, "Propagation of a solitary wave over a finite submerged thin plate," *Applied Ocean Research*, vol. 106, p. 102425, 2021.
[18] Y. Yang, S. Draycott, P. K. Stansby, and B. D. Rogers, "A numerical flume for waves on variable sheared currents using smoothed particle hydrodynamics (SPH) with open boundaries," *Applied Ocean Research*, vol. 135, p. 103527, 2023.
[19] I. Afgan, J. McNaughton, S. Rolfo, D. D. Apsley, T. Stallard, and P. Stansby, "Turbulent flow and loading on a tidal stream turbine by LES and RANS," *International Journal of Heat and Fluid Flow*, vol. 43, pp. 96–108, 2013.
[20] A. Posa and R. Broglia, "Characterization of the turbulent wake of an axial-flow hydrokinetic turbine via large-eddy simulation," *Computers and Fluids*, vol. 216, p. 104815, 2021.
[21] P. Ouro, L. Ramírez, and M. Harrold, "Analysis of array spacing on tidal stream turbine farm performance using Large-Eddy Simulation," *Journal of Fluids and Structures*, vol. 91, p. 102732, 2019.
[22] P. Ouro, H. Mullings, and T. Stallard, "Establishing confidence in predictions of fatigue loading for floating tidal turbines based on large-eddy simulations and unsteady blade element momentum," in *5th International Conference on Renewable Energies Offshore, RENEW 2022*, 2022, pp. 915–924.
[23] A. Posa and R. Broglia, "Analysis of the momentum recovery in the wake of aligned axial-flow hydrokinetic turbines," *Physics of Fluids*, vol. 34, p. 105130, 2022.
[24] F. Nicoud and F. Ducros, "Subgrid-scale stress modelling based on the square of the velocity," *Flow Measurement and Instrumentation*, vol. 62, pp. 183–200, 1999.
[25] P. Ouro, U. Lopez-Novoa, and M. F. Guest, "On the performance of a highly-scalable Computational Fluid Dynamics code on AMD, ARM and Intel processor-based HPC systems," *Computer Physics Communications*, vol. 269, p. 108105, 2021.
[26] P. Ouro and T. Nishino, "Performance and wake characteristics of tidal turbines in an infinitely large array," *Journal of Fluid Mechanics*, vol. 925, pp. 1–32, 2021.
[27] T. Stallard, T. Feng, and P. K. Stansby, "Experimental study of the mean wake of a tidal stream rotor in a shallow turbulent flow," *Journal of Fluids and Structures*, vol. 54, pp. 235–246, 2015.
[28] N. Jarrin, S. Benhamadouche, D. Laurence, and R. Prosser, "A synthetic-eddy-method for generating inflow conditions for large-eddy simulations," *International Journal of Heat and Fluid Flow*, vol. 27, pp. 585–593, 2006.
[29] S. Kang, I. Borazjani, J. A. Colby, and F. Sotiropoulos, "Numerical simulation of 3D flow past a real-life marine hydrokinetic turbine," *Advances in Water Resources*, vol. 39, pp. 33–43, 2012.
[30] P. Ouro, M. Harrold, T. Stoesser, and P. Bromley, "Hydrodynamic loadings on a horizontal axis tidal turbine prototype," *Journal of Fluids and Structures*, vol. 71, pp. 78–95, 2017.